ILASS-Americas 22nd Annual Conference on Liquid Atomization and Spray Systems, Cincinnati, OH, May 2010

The Influence of Density Ratio on the Primary Atomization of a Turbulent Liquid Jet in Crossflow

M. Herrmann*
School of Mechanical, Aerospace, Chemical, and Materials Engineering
Arizona State University, Tempe, AZ 85287

Abstract

In this paper we study the impact of density ratio on the liquid jet in crossflow penetration, deformation, and atomization if all other characteristic parameters, i.e. momentum flux ratio, jet and crossflow Weber and Reynolds numbers, are maintained constant. We perform detailed simulations of the primary atomization region using the refined level set grid method to track the motion of the liquid/gas phase interface. We employ a balanced force, interface projected curvature method to ensure high accuracy of the surface tension forces, use a multi-scale approach to transfer broken off, small scale nearly spherical drops into a Lagrangian point particle description allowing for full two-way coupling and continued secondary atomization, and employ a dynamic Smagorinsky large eddy simulation approach in the single phase regions of the flow to describe turbulence. We compare simulation results obtained previously using a liquid to gas density ratio of 10 for a momentum flux ratio 6.6, Weber number 330, and Reynolds number 14000 liquid jet injected into a Reynolds number 740,000 gaseous crossflow to those at a density ratio of 100, a value typical for gas turbine combustors. The results show that the increase in density ratio results in a noticeable increase in jet penetration and decrease in liquid core deformation in the transverse direction.

*Corresponding Author: marcus.herrmann@asu.edu

Introduction

The atomization of turbulent liquid jets injected into fast moving, subsonic gaseous crossflows is an important application for example in gas turbines, ramjets, and augmentors. It is a highly complex process, that has been extensively studied experimentally over the past decades. Early studies of the atomization of non-turbulent liquid jets in crossflows have recently been reviewed in [1], whereas newer studies of this case include the work reported in [2, 3, 4, 5, 6, 7, 8, 9, 10, 11, 12]. Most experimental work has focused on jet penetration, including both the column trajectory and the resulting spray penetration under ambient, atmospheric conditions. Some recent jet penetration correlations under these conditions can be found in [3, 10, 11, 12]. Under non-atmospheric conditions, jet penetration correlations have been derived in [2, 13]. The identified characteristic parameters determining jet penetration from these studies are the momentum flux ratio [12], momentum flux ratio and crossflow Weber number [11], momentum flux ratio and water to injected liquid viscosity ratio [3], momentum flux ratio, crossflow Weber number, and water to injected liquid viscosity ratio [10], momentum flux ratio, crossflow Weber and Reynolds numbers [2], and momentum flux ratio, crossflow Weber number, and channel pressure [13]. Since gaseous density is proportional to channel pressure, only the latter correlation contains the impact of density ratio on liquid jet penetration directly. However, although momentum flux ratio and crossflow and jet Weber numbers were approximately held constant, at least one of the Reynolds numbers could not have been maintained, thus potentially overlapping two separate effects. It should be pointed out that some other studies exist that vary the channel pressure from its atmospheric value, however, these studies consider modified configurations, for example airblast assisted atomization [14], or did not result in modifications to the liquid jet core penetration correlations [15].

All the above studies at non-atmospheric conditions use as a starting point correlations obtained at atmospheric conditions, since their is an abundance of data there. Density ratios found in applications like gas turbine combustors are thus approached from above, i.e. atmospheric conditions result in too large density ratios and non-atmospheric experiments analyze the effect of increasing the crossflow channel pressure and thereby reducing the density ratio in steps to those values representative of gas turbine combustors [13]. One question addressed is thus how representative are experiments at atmospheric conditions of the actual application?

Detailed numerical simulations of turbulent atomization processes, on the other hand, are typically performed at density ratios smaller than those found in gas turbine combustors due to often times encountered numerical instabilities associated with the density discontinuity on highly deformed interfaces. The question we thus aim to address here is how representative are those simulations at lower density ratio conditions of the actual application in terms of jet penetration?

The outline of this paper is the following: after summarizing the governing equations, the numerical methods employed to solve them are briefly outlined. Then, simulation results are presented and the impact of density ratio on jet penetration is discussed.

Governing equations

The equations governing the motion of an unsteady, incompressible, immiscible, two-fluid system are the Navier-Stokes equations,

$$\begin{aligned} \frac{\partial \boldsymbol{u}}{\partial t} &+ \boldsymbol{u}\cdot\nabla\boldsymbol{u} = -\frac{1}{\rho}\nabla p \\ &+ \frac{1}{\rho}\nabla\cdot\left(\mu\left(\nabla\boldsymbol{u}+\nabla^T\boldsymbol{u}\right)\right)+\frac{1}{\rho}\boldsymbol{T}_\sigma\,, \end{aligned} \quad (1)$$

where $\boldsymbol{u}$ is the velocity, ρ the density, p the pressure, μ the dynamic viscosity, and $\boldsymbol{T}_\sigma$ the surface tension force which is non-zero only at the location of the phase interface $\boldsymbol{x}_f$. Furthermore, the continuity equation results in a divergence-free constraint on the velocity field, $\nabla\cdot\boldsymbol{u}=0$. The phase interface location $\boldsymbol{x}_f$ between the two fluids is described by a level set scalar G, with $G(\boldsymbol{x}_f,t)=0$ at the interface, $G(\boldsymbol{x},t)>0$ in fluid 1, and $G(\boldsymbol{x},t)<0$ in fluid 2. Differentiating this with respect to time yields,

$$\frac{\partial G}{\partial t}+\boldsymbol{u}\cdot\nabla G=0\,. \quad (2)$$

Assuming material properties to be constant within each fluid, they can be calculated at any point $\boldsymbol{x}$ from

$$\alpha(\boldsymbol{x})=H(G)\alpha_1+(1-H(G))\alpha_2 \quad (3)$$

where α is either density or viscosity, indices 1 and 2 denote values in fluid 1, respectively 2, and H is the Heaviside function. From the definition of the level set scalar G it follows that

$$\delta(\boldsymbol{x}-\boldsymbol{x}_f)=\delta(G)|\nabla G| \quad (4)$$

with δ the Dirac delta function. Furthermore, the interface normal vector $\boldsymbol{n}$ and the interface curvature κ can be expressed in terms of the level set scalar as

$$\boldsymbol{n}=\frac{\nabla G}{|\nabla G|}\,,\quad \kappa=\nabla\cdot\boldsymbol{n}\,. \quad (5)$$

Using Eqs. (4) and (5), the surface tension force $\boldsymbol{T}_\sigma$ can thus be expressed as

$$\boldsymbol{T}_\sigma(\boldsymbol{x}) = \sigma\kappa\delta(\boldsymbol{x}-\boldsymbol{x}_f)\boldsymbol{n} = \sigma\kappa\delta(G)|\nabla G|\boldsymbol{n}\,, \qquad (6)$$

with σ the surface tension coefficient.

Numerical methods

To keep track of the position and motion of the phase interface, we solve all level set related equations using the Refined Level Set Grid (RLSG) on a separate, equidistant Cartesian grid using a dual-narrow band methodology for efficiency. This so-called G-grid is overlaid onto the flow solver grid on which the Navier-Stokes equations are solved and can be independently refined, providing high resolution of the tracked phase interface geometry. Details of the method and the resulting level set solver LIT, i.e. narrow band generation, level set transport, re-initialization, curvature evaluation, as well as its performance compared to other interface tracking methods in generic advection test cases can be found in [16].

In the Navier-Stokes equations, the position of the phase interface influences two different terms. The first term is due to Eq. (3), since $H(G)$ is a function of the position of the phase interface. For finite volume formulations, the volume fraction ψ_{cv} of a control volume is defined as

$$\psi_{cv} = 1/V_{cv}\int_{V_{cv}} H(G)dV\,, \qquad (7)$$

with V_{cv} the volume of the control volume cv. In the RLSG method, the above integral is evaluated using the high-resolution G-grid [16]. Then control volume material properties are simply

$$\alpha_{cv} = \psi_{cv}\alpha_1 + (1-\psi_{cv})\alpha_2\,. \qquad (8)$$

The second term that is a function of the interface position is the surface tension force term, Eq. (6). Here it is critical for stability and accuracy, that the surface tension force can be balanced by the pressure gradient (jump) across the phase interface exactly on the discrete level. This is ensured by the balanced force approach [16, 17] based on the Continuum Surface Force (CSF) model [18]. The phase interface curvature κ is calculated on the high-resolution G-grid, using a second order accurate interface projected curvature calculation method [16].

The flow solver used to solve the incompressible two-phase Navier-Stokes equations on unstructured grids using the finite volume balanced force algorithm is Cascade Technologies' CDP. In the single phase regions, the employed scheme conserves the kinetic energy discretely and turbulence is modeled using a dynamic Smagorinsky LES model. However, none of the terms arising from filtering the phase interface are modeled. The approach instead relies on resolving all relevant scales at the phase interface, thus ideally reverting to a DNS at the phase interface. As such, the current simulation approach is a combination of LES in the single phase regions and ideally DNS at the phase interface [19].

The flow solver CDP and the interface tracking software LIT are coupled using the parallel multi-code coupling library CHIMPS [16, 20]. In order to couple the level set equation to the Navier-Stokes equation, $\boldsymbol{u}$ in Eq. (2) is calculated from the flow solver velocity by tri-linear interpolation. To achieve overall second-order accuracy in time, the level set equation is solved staggered in time with respect to the Navier-Stokes equations.

Finally, resolving the entire phase interface geometry by tracking the phase interface associated with each atomized drop quickly becomes prohibitively expensive. Instead, we follow a multi-scale coupled Eulerian/Lagrangian procedure in that we track the phase interface by the Eulerian level set method in the near injector primary atomization region and transfer broken-off, nearly spherical liquid structures into a Lagrangian point particle description [21]. In the Lagrangian description, full two-way momentum coupling between the drop and continuous phase is used [22], including a stochastic secondary atomization model [23]. However, the cell volume occupied by the Lagrangian drops is not explicitly taken into account and neither drop/drop nor drop/tracked phase interface collisions are modeled. But, as long as liquid structures have not been transferred into the Lagrangian description, i.e. they are still tracked by the level set scalar, secondary breakup, cell volume effects, and all collisions are fully captured.

Computational Domain and Operating Conditions

The case analyzed in this paper is one studied experimentally by Brown & McDonell [4]. Table 1 summarizes the operating conditions and resulting characteristic numbers. Results obtained for the density ratio 10 case were reported previously in [19, 24].

The computational domain ($-25D\ldots50D \times 0\ldots25D \times -10D\ldots10D$) is smaller than the channel used in the experiment ($-77D\ldots127D \times 0\ldots54D \times -27D\ldots27D$). However, simulations using the full experimental channel geometry were conducted to verify that the reduced computational

	sim. 1	sim. 2
density ratio $R = \rho_j/\rho_c$	10	100
jet exit diameter D [mm]	1.3	1.3
crossflow density ρ_c [kg/m^3]	1.225	1.225
jet density ρ_j [kg/m^3]	12.25	122.25
crossflow velocity u_c [m/s]	1 120.4	120.4
jet velocity u_j [m/s]	1 97.84	30.94
crossflow viscosity μ_c [kg/ms]	1.82 e-5	1.82e-5
jet viscosity μ_j [kg/ms]	1.11e-4	3.5e-4
surface tension coeff. σ [N/m]	0.07	0.07
momentum flux ratio q	6.6	6.6
crossflow Weber number We_c	330	330
jet Weber number We_j	2178	2178
crossflow Reynolds number Re_c	5.7e5	5.7e5
jet Reynolds number Re_j	14079	14079

Table 1. Operating conditions and characteristic numbers.

domain does not impact the reported results. Furthermore, the details of the injector geometry are taken into account by performing at a constant momentum flux ratio a turbulent single phase LES of the full geometry and storing the resulting velocities in a database for use as the injector exit-plane inflow boundary condition in the atomization simulations [19, 24].

We previously reported on a grid refinement study for the $\rho_j/\rho_c = 10$ case using three different grid resolutions [19, 24]. The obtained results indicate that jet penetration can be well predicted even on the coarsest grid, column and surface breakup modes can be observed on all three grids, and that grid independent drops resulting from primary atomization can be obtained for drops resolved by at least 2 grid nodes of the RLSG grid. Thus, in the following, we will limit ourselves to only one grid resolution, the medium resolution grid c12 used in [19, 24]. It resolves the injector diameter by 32 control volumes using a static mesh refinement strategy in the injector region in the flow solver, see Fig. 1 and 64 grid nodes in the RLSG solver. The resulting mesh sizes are 21 million control volumes for the flow solver and 13 million active RLSG grid nodes. At $t = 0$, the liquid jet is initialized in the computational domain by a small cylindrical section of length D capped by a half-sphere, protruding into the crossflow channel.

In the following, unless otherwise indicated, results are reported in dimensionless quantities, with $\boldsymbol{u}_j$ and D being the reference velocity and length. Thus, non-dimensional coordinates are the same in both density cases, whereas non-dimensional times and velocities are different by a factor 3.16.

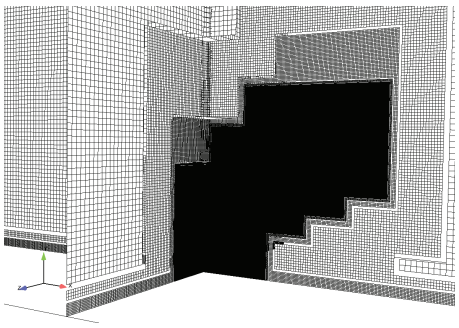

Figure 1. Mesh detail near the injector.

Results and Discussion

Figure 2 compares instantaneous snapshots of the surface geometry for the two different density ratios. Jet penetration appears different, with the higher density case being less bent in the crossflow direction, and the liquid core not extending as far in that direction.

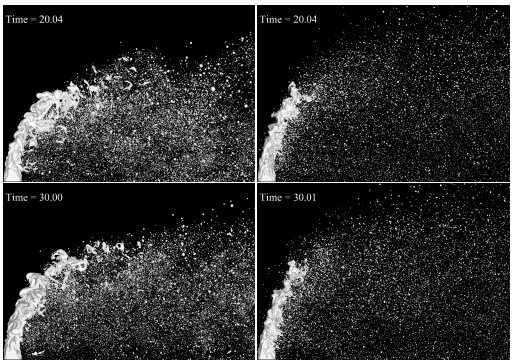

Figure 2. Side view snapshots of jet in crossflow atomization at t=20 (top) and 30 (bottom) time units, $\rho_j/\rho_c = 10$ (left) and 100 (right).

To allow for a detailed quantitative analysis of the mean jet penetration, the following procedure is adopted to extract such data from time snapshots of the level set solution field. Since the interest here is on time averaged data, it should be pointed out that a simple time averaging of the level set scalar is doomed to fail and give inaccurate results, since such an approach violates the inherent symmetries of the level set equation [25]. Instead, we base our averaging tool on the spatial filters for level set scalars proposed in [26], applied to temporal filtering instead of spatial filtering. The idea in this approach is to perform the averaging on a Heaviside transform of the level set scalar instead of on the level set scalar

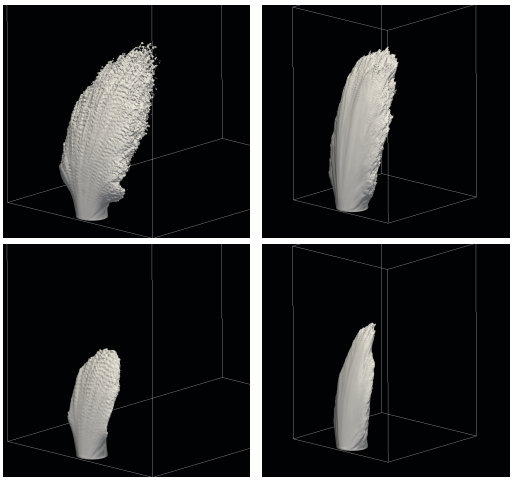

Figure 3. Impact of density ratio on probability threshold of finding liquid, 10% probability (top) and 50%, probability (bottom) for $\rho_j/\rho_c = 10$ (left) and 100 (right).

itself. This, in essence, results in a scalar that describes the threshold probability of finding liquid at a given location (the probability is x% or greater). Additionally, this scalar is consistent with a mean liquid volume fraction. In principle, any value of the resulting scalar can be used to identify the position of the mean surface. A natural choice would be the 50% probability iso-surface, but any other value can be used as well. Figure 3 shows the probability iso-surfaces of 10% and 50% for finding the liquid core for the two density ratios. The lower density ratio case exhibits significantly more expansion in the transverse direction, whereas the higher density ratio results in a more upright, compact liquid core. This observation is supported by Fig. 4,

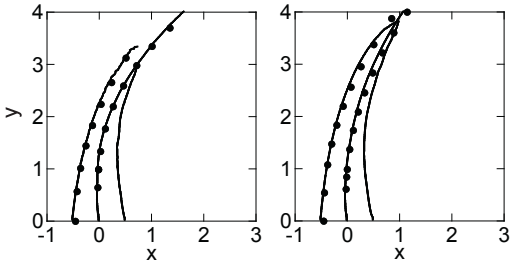

Figure 4. Center of mass, windward and lee side 50% probability isoline in the injector midplane. Symbols are power law fits. $\rho_j/\rho_c = 10$ (left) and 100 (right).

which presents the position of the liquid core's center of mass and windward and lee-side 50% probability iso-lines in the injector's center plane. The center of mass position was determined by an iterative procedure evaluating the center of mass in planes normal to its trajectory. Also shown are power law fits, where $y/D = 3.3(x/D)^{0.33}$ and $y/D = 3.8(x/D)^{0.40}$ fit the center of mass trajectory in the low and high density ratio case, respectively. The 50% probability leading edge can be fitted by $y/D = 3.18(x/D)^{0.49}$, respectively $y/D = 3.4(x/D)^{0.45}$. The power law fits obtained from experiments are $y/D = 3.5(x/D)^{0.50}$ [12] and $y/D = 3.6(x/D)^{0.39}$ [27].

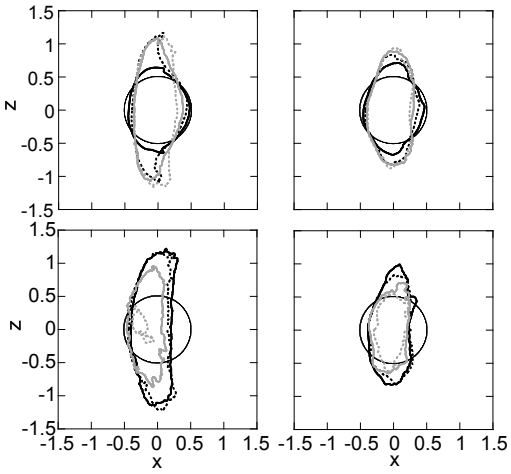

Figure 5. 20% probability surface at $y/D = 0$ (thin black), 0.5 (top, black), 1.0 (top, black dotted), 1.5 (top, gray), 2.0 (top, gray dotted), 2.5 (bottom, black), 3.0 (bottom, black dotted), 3.5 (bottom, gray), and 4.0 (bottom, gray dotted) for $\rho_j/\rho_c = 10$ (left) and 100 (right).

Figure 5 shows the 20% probability iso-lines of finding liquid in different cut planes normal to the jet's center of mass trajectory at varying heights above the injector exit. The origin in these plots corresponds to the jet's center of mass. It has been hypothesized in the recent past that a non-turbulent liquid jet in a uniform crossflow deforms and breaks similar to the secondary breakup of drops subjected to shock wave disturbances [8, 12, 28]. Simulation results based on this premise have been reported in [1]. Our simulation results show that the lower density ratio case leads to a quick deformation of the initially circular cross section at the injector exit exhibiting small deformations on the sides reminiscent of a drop stripping mode. Starting at $y/D = 2.0$ the jet indeed shows deformation characteristics typical of drops subjected to crossflows.

In the higher density ratio case, the jet is prone

to much less deformation. No bending of the profiles in the crossflow direction near the jet's sides is observed as in the low density ratio case. This result is in disagreement with the model results reported in [1]. There, an increase in density ratio results in an increase in deformation which is contrary to our observation. This seeming discrepancy might be due to the difference in Weber numbers used, We = 4 [1] versus We = 330 used here, or due to the presence of turbulence and/or three-dimensional effects.

Acknowledgments

This work was supported in part by CASCADE Technologies Inc. under NavAir SBIR N07-046. The author would like to thank M. Arienti and M. Soteriou from United Technologies Research Center for many helpful discussions and participation in the NavAir SBIR as well as S. Hajiloo and F. Ham from Cascade Technologies Inc.

References

[1] C. Aalburg, B. van Leer, G. M. Faeth, K. A. Sallam, Properties of nonturbulent round liquid jets in uniform gaseous cross flows, Atom. Sprays 15 (3) (2005) 271–294.

[2] A. Bellofiore, A. Cavaliere, R. Ragucci, Air density effect on the atomization of liquid jets in crossflow, Combust. Sci. and Tech. 179 (1-2) (2007) 319–342.

[3] M. Birouk, C. O. Iyogun, N. Popplewell, Role of viscosity on trajectory of liquid jets in a cross-airflow, Atom. Sprays 17 (3) (2007) 267–287.

[4] C. T. Brown, V. G. McDonell, Near field behavior of a liquid jet in a crossflow, in: ILASS Americas, 19th Annual Conference on Liquid Atomization and Spray Systems, Toronto, Canada, 2006.

[5] C. T. Brown, U. M. Mondragon, V. G. McDonell, Investigation of the effect of injector discharge coefficient on penetration of a plain liquid jet into a subsonic crossflow, in: ILASS Americas 20th Annual Conference on Liquid Atomization and Spray Systems, ILASS Americas, Chicago, IL, 2007.

[6] R. P. Fuller, P.-K. Wu, K. A. Kirkendall, A. S. Nejad, Effects of injection angle on atomizationof liquid jets in transverse ai, AIAA J. 38 (1) (2000) 64–72.

[7] K. Lee, C. Aalburg, F. J. Diez, G. M. Faeth, K. A. Sallam, Primary breakup of turbulent round liquid jets in uniform crossflows, AIAA J. 45 (8) (2007) 1907–1916.

[8] J. Mazallon, Z. Dai, G. M. Faeth, Primary breakup of nonturbulent round liquid jets in gas crossflows, Atom. Sprays 9 (3) (1999) 291–311.

[9] C. L. Ng, R. Sankarakrishnan, K. A. Sallam, Bag breakup of nonturbulent liquid jets in crossflow, International Journal of Multiphase Flow 34 (3) (2008) 241–259.

[10] J. N. Stenzler, J. G. Lee, D. A. Santavicca, W. Lee, Penetration of liquid jets in a crossflow, Atom. Sprays 16 (2006) 887–906.

[11] S. M. Thawley, U. M. Mondragon, C. T. Brown, V. G. McDonell, Evaluation of column breakpoint and trajectory for a plain liquid jet injected into a crossflow, in: Proceedings of the 21st Annual Conference on Liquid Atomization and Spray Systems, ILASS Americas, Orlando, FL, 2008, pp. 1–11.

[12] P. K. Wu, K. A. Kirkendall, R. P. Fuller, A. S. Nejad, Breakup processes of liquid jets in subsonic crossflows, J. Propul. Power 13 (1) (1997) 64–73.

[13] O. M. Elshamy, Experimental investigations of steady and dynamic behavior of transverse liquid jets, Ph.D. thesis, University of Cincinnati (2007).

[14] M. Y. Leong, V. G. McDonell, G. S. Samuelsen, Effect of ambient pressure on an airblast spray injected into a crossflow, J. Propul. Power 17 (5) (2001) 1076–1084.

[15] J. Becker, C. Hassa, Breakup and atomization of a kerosene jet in crossflow at elevated pressure, Atom. Sprays 11 (2002) 49–67.

[16] M. Herrmann, A balanced force refined level set grid method for two-phase flows on unstructured flow solver grids, J. Comput. Phys. 227 (4) (2008) 2674–2706.

[17] M. M. Francois, S. J. Cummins, E. D. Dendy, D. B. Kothe, J. M. Sicilian, M. W. Williams, A balanced-force algorithm for continuous and sharp interfacial surface tension models within a volume tracking framework, J. Comput. Phys. 213 (2006) 141–173.

[18] J. U. Brackbill, D. B. Kothe, C. Zemach, A continuum method for modeling surface tension, J. Comput. Phys. 100 (1992) 335–354.

[19] M. Herrmann, Detailed numerical simulations of the primary atomization of a turbulent liquid jet in crossflow, Journal of Engineering for Gas Turbines and Power 132 (6) (2010) 061506–10.

[20] J. J. Alonso, S. Hahn, F. Ham, M. Herrmann, G. Iaccarino., G. Kalitzin, P. LeGresley, K. Mattsson, G. Medic, P. Moin, H. Pitsch, J. Schluter, M. Svard, E. V. der Weide, D. You, X. Wu, CHIMPS: A high-performance scalable module for multi-physics simulation, in: 42nd AIAA/ASME/SAE/ASEE Joint Propulsion Conference & Exhibit, no. 2006-5274 in AIAA-Paper, 2006.

[21] M. Herrmann, A parallel eulerian interface tracking/lagrangian point particle multi-scale coupling procedure, J. Comput. Phys. 229 (2010) 745–759.

[22] P. Moin, S. V. Apte, Large-eddy simulation of realistic gas turbine combustors, AIAA J. 44 (4) (2006) 698–708.

[23] S. V. Apte, M. Gorokhovski, P. Moin, Les of atomizing spray with stochastic modeling of secondary breakup, Int. J. Multiphase Flow 29 (9) (2003) 1503–1522.

[24] M. Herrmann, Detailed numerical simulations of the primary atomization of a turbulent liquid jet in crossflow, in: Proceedings ASME Turbo Expo 2009: Power for Land, Sea and Air, no. GT2009-59563, 2009.

[25] M. Oberlack, H. Wenzel, N. Peters, On symmetries and averaging of the G-equation for premixed combustion, Combust. Theory Modelling 5 (2001) 363–383.

[26] M. Herrmann, DNS of turbulent primary atomization using a level set/vortex sheet method, in: ILASS Americas 18th Annual Conference on Liquid Atomization and Spray Systems,Irvine, CA, 2005.

[27] J. N. Stenzler, J. G. Lee, D. A. Santavicca, Penetration of liquid jets in a cross-flow, in: 41st Aerospace Sciences Meeting and Exhibit, no. AIAA 2003-1327 in AIAA-Paper, 2003.

[28] K. A. Sallam, C. Aalburg, G. M. Faeth, Breakup of round nonturbulent liquid jets in gaseous crossflow, AIAA J. 42 (12) (2004) 2529–2540.